ACS APPLIED POLYMER MATERIALS

pubs.acs.org/acsapm Article

Lower Critical Solution Temperature-Driven Catch and Release of Perfluoroalkyl Substances from Water: Remediation and Sampling

Mohammadamin Ezazi, Bishwash Shrestha, and Gibum Kwon*

Cite This: *ACS Appl. Polym. Mater.* 2021, 3, 4139−4146 Read Online

ACCESS | Metrics & More | Article Recommendations | Supporting Information

ABSTRACT: Water pollution by per- and polyfluoroalkyl substances (PFASs) is a rising issue for the environment and human health because PFASs are persistent and nonbiodegradable. Recent studies have revealed that the concentration of PFASs found in contaminated water is in the order of the parts per trillion (i.e., 10^{-12}) scale. This can result in a grand challenge for scientists not only to remove PFASs from water but to detect them. Various methodologies including functionalized nanoparticles, bioassay, activated carbon, anion exchange resin, and molecularly imprinted polymers have been employed to detect or remove PFASs from water. Dynamic adsorbents have demonstrated that they can adsorb PFASs from water while releasing them on demand for reuse upon an external trigger. This enables one to remove PFASs from water and retain them for preconcentration, while on-demand releasing allows for regenerating the adsorbent for reuse. Herein, a poly(isopropylmethacrylamide) (P-NIPMAM)-based adsorbent that can adsorb and retain PFASs at a temperature higher than its lower critical solution temperature (LCST) while releasing them at a lower temperature is reported. Perfluorooctanoic acid (PFOA) and perfluorohexanoic acid (i.e., PFHxA) are utilized as a representative PFAS with a long and short fluoroalkyl chain, respectively. The adsorption capacity for PFOA and PFHxA is measured as ≈37 and ≈18 mg g^{-1} at 75 °C, respectively. When the adsorbent is submerged in water at a lower temperature (e.g., 23 °C < LCST), it starts to release the adsorbed compounds resulting in the desorption efficiency of ≈0.66 and ≈0.81 for PFOA and PFHxA, respectively. Finally, a prototype PFAS sampler was engineered by utilizing P-NIPMAM that can demonstrate the LCST-driven reversible adsorption and desorption of PFASs.

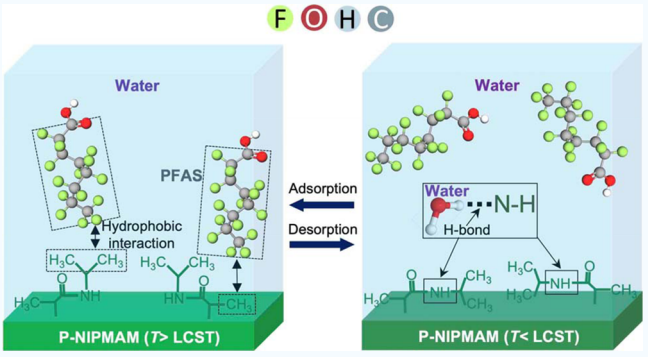

KEYWORDS: *perfluoroalkyl substances, poly(isopropylmethacrylamide), dynamic adsorbent, reversible adsorption and desorption, sampling, water remediation*

INTRODUCTION

Per- and polyfluoroalkyl substances (PFASs) are a class of organofluorines that have been utilized in a wide range of applications including surfactants,[1] aqueous film-forming foams,[2] and oleophobic coatings[3] due to their excellent thermal stability,[4] low surface free energy,[5] and chemical inertness.[6] Recent reports[7−10] have revealed that PFASs are found in soil or groundwater in various places such as the sites at which firefighting activities have undertaken and industrial effluents have been disposed. Paradoxically, their excellent chemical durability and thermal stability make PFASs persistent in both the environment and the human body.[11] While it remains an active research topic, it is generally agreed that PFASs can cause a variety of human health disorders and pose adverse effects to both aquatic and terrestrial ecosystems.[12] In accordance with these findings, the U.S. Environmental Protection Agency (EPA) included perfluorooctanoic acid (PFOA) and perfluorosulfonic acid (PFOS) in the List of Contaminant Candidate issued in the 2016 annual report.[13] More recently, the U.S. Drinking Water Health Advisory restricted the PFAS concentration in drinking water to 70 parts per trillion (ppt) or less.[4,14]

One of the prevailing methods to measure the PFAS concentration in water is using ultrahigh-performance liquid chromatography (UHPLC).[15,16] A typical limit of detection (LoD, i.e., lowest concentration of a contaminant that can be reliably detected) is 10−60 ppt.[17] Given that the PFAS concentration of groundwater or soil found in the contaminated sites can be as low as ≈10 ppt level,[18] both detecting and removing such trace amounts of PFAS is a grand challenge. To enhance the detection limit, an ultrasensitive nanosensor has been reported as an emerging tool for detecting PFASs at a low LoD (e.g., <10 ppt). For example, Zhang et al.[19] synthesized

Received: May 19, 2021
Accepted: July 26, 2021
Published: August 4, 2021

https://doi.org/10.1021/acsapm.1c00608
ACS Appl. Polym. Mater. 2021, 3, 4139−4146

magnetite (Fe_3O_4) nanoparticles functionalized by octadecyltriethoxysilane and chitosan derivative compounds. The resulting Fe_3O_4 nanoparticles can concentrate PFASs (e.g., perfluoroundecanoic acid and perfluorododecanoic acid) at a concentration as low as ≈0.075 ppt (i.e., 0.075 ng L^{-1}) in water. Xia et al.[20] developed a bioassay to detect trace amounts of PFASs via ligand−receptor interaction by utilizing functionalized gold nanoparticles. The LoD of the bioassay for PFOS was ≈5.0 ppt (10 pM). Chen et al.[21] developed an electrochemiluminescence sensor that can detect PFOA using polypyrrole-modified carbon nitride (C_3N_4) nanosheets. The sensor can detect PFOA with an LoD of ≈10 ppt. Furthermore, Li et al.[22] developed a sensor based on an ion-selective electrode that can detect PFOS and perfluorooctanoate (PFO^-) with an LoD of ≈430.0 and ≈70.0 ppt, respectively.

Recently, dynamic adsorbents have demonstrated that they can not only detect PFASs but also release them on demand for regeneration or reuse.[23−25] For example, Ateia et al.[23] synthesized a hydrogel using poly(*N*-[3-(dimethylamino)-propyl]acrylamide, methyl chloride quaternary) that can adsorb PFASs from water, while it can release it to an aqueous solution containing sodium chloride (NaCl, 1.0%) and methanol (30:70, vol/vol). Saad et al.[24] leveraged the low critical solution temperature (LCST) behavior of poly-*N*-isopropylacrylamide (PNIPAm) to adsorb and desorb PFASs upon a temperature change. When a temperature is higher than the LCST, the isopropyl groups can be dehydrated resulting in adsorption for PFASs via interacting with its hydrophobic tail. Upon a decrease in temperature below the LCST, PFASs can be desorbed from PNIPAm. More recently, Xiang et al.[25] synthesized phenolic resin microspheres coated with PFOA and polyethylene glycol (PEG). PFOA can selectively catch the fluorinated compounds, while PEG can enhance the wettability of microspheres to water. When a temperature is above the LCST of PEG, the captured fluorinated pollutants could be readily separated from water.

Herein, a thermoresponsive poly(isopropylmethacrylamide) (P-NIPMAM) is reported that can exhibit reversible adsorption and desorption of PFAS from water upon switching temperature. The LCST of P-NIPMAM was measured as ≈73.9 °C. PFOA and perfluorohexanoic acid (i.e., PFHxA) were utilized as representative PFASs with a long and short fluoroalkyl chain, respectively. The adsorption capacity for PFOA and PFHxA was measured as ≈37 and ≈18 mg g^{-1} at 75 °C, respectively. When the temperature became ≈23 °C, lower than the LCST, the adsorbed PFOA and PFHxA were desorbed with a desorption efficiency of ≈0.66 and ≈0.81, respectively. A higher adsorption capacity and a lower desorption efficiency for PFOA in comparison with PFHxA can be attributed to a stronger hydrophobic interaction with a longer fluoroalkyl chain. Finally, a prototype PFAS sampler was engineered by utilizing P-NIPMAM that can demonstrate the LCST-driven reversible adsorption and desorption of PFASs.

RESULTS AND DISCUSSION

P-NIPMAM was prepared by free-radical polymerization of NIPMAM in a mixture of water and ethanol (80:20, vol/vol) at 70 °C. Here, potassium persulfate (KPS) and *N*,*N*′-methylenebisacrylamide (MBAA) were used as an initiator and a cross-linker, respectively (Figure 1a). The initiator (anionic sulfate groups)[26] can react with carbon−carbon double bonds (e.g., $H_2C{=}C(CH_3)$ or $H_2C{=}CH$) in an acrylate group of NIPMAM and MBAA resulting in cross-linked P-NIPMAM. The P-NIPMAM was then rinsed with deionized (DI) water to remove unreacted monomers followed by drying in a vacuum oven at 70 °C for 3 h (Experimental Section).

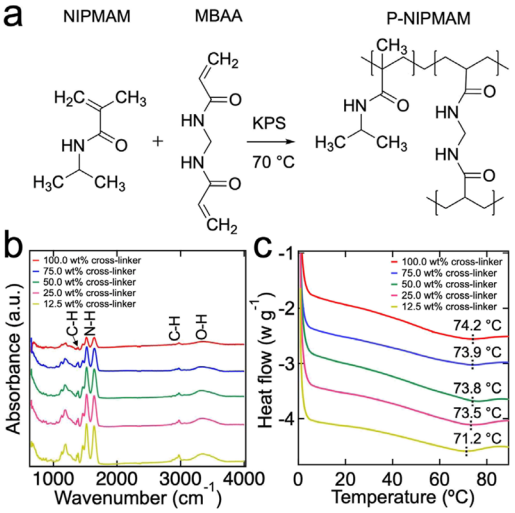

Figure 1. (a) Synthesis of P-NIPMAM by a temperature-driven free-radical polymerization of the NIPMAM monomer, MBAA as a cross-linker, and KPS as an initiator. (b,c) FTIR spectra (b) and DSC curves of heat flow (c) for P-NIPMAM prepared with cross-linker concentrations in the range of 12.5−100.0 wt % with respect to the mass of the NIPMAM monomer. The peaks indicated by dotted lines demonstrate the LCST.

The P-NIPMAM's surface chemistry was characterized by Fourier-transform infrared (FTIR) spectroscopy (Figure 1b). Here, P-NIPMAMs were prepared with varying cross-linker concentrations (e.g., 12.5, 25.0, 50.0, 75.0, and 100.0 wt % with respect to the mass of NIPMAM monomer). A broad absorption band at ≈3400 cm^{-1} corresponds to the O−H stretching vibrations, while the bands at ≈1550 and ≈1640 cm^{-1} are assigned to the N−H stretching vibration of amide II and C═O stretching mode of amide I, respectively.[27−29] The absorption bands at ≈1380, ≈1440, and ≈1460 cm^{-1} are assigned to C−H deformation, while those at ≈2870, ≈2930, and ≈2960 cm^{-1} correspond to the symmetric and asymmetric stretching vibration of C−H bonds, respectively.[28] Of note, the intensity of a characteristic band at ≈2930 cm^{-1} (i.e., ═C−H bond) slightly decreases with an increase in the cross-linker concentration. This indicates a higher degree of cross-linking of the carbon−carbon double bonds which are the main cross-linking points in P-NIPMAM.[30]

As a thermoresponsive polymer, P-NIPMAM exhibits an LCST behavior. When a temperature is below the LCST, the P-NIPMAM network exists in an extended coil-like conformation exposing its hydrophilic groups (i.e., −NH).[31−34] When a temperature becomes above the LCST, the solvation entropy of hydrophobic groups (i.e., methyl and isopropyl groups) becomes dominant resulting in globule-like collapsed conformation.[33,35,36] The LCST values were measured by conducting differential scanning calorimetry (DSC) (Experimental Section). Figure 1c demonstrates the endothermic heating curves for P-NIPMAMs prepared with varying cross-linker concentrations. The LCST values were measured as ≈71.2, ≈73.5, ≈73.8, ≈73.9, and ≈74.2 °C for the P-NIPMAM prepared with 12.5, 25.0, 50.0, 75.0, and 100.0 wt

https://doi.org/10.1021/acsapm.1c00608
ACS Appl. Polym. Mater. 2021, 3, 4139−4146

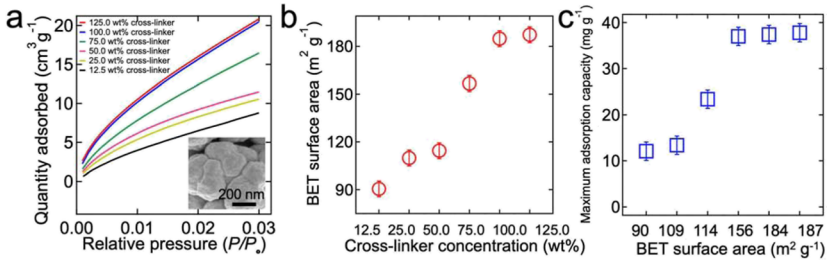

Figure 2. (a) BET plots determined by utilizing CO_2 adsorption isotherms at 273 °K. The inset shows a SEM image of P-NIPMAM prepared with 75.0 wt % of the cross-linker. (b) Measured BET surface area as a function of cross-linker concentration. (c) Measured maximum adsorption capacity for PFOA in DI water (C_o = 0.6 mg mL^{-1}) as a function of BET surface area.

% of the cross-linker, respectively. An increase in the LCST value of P-NIPMAM prepared with a higher cross-linker concentration can be attributed to topological constraints caused by an increase in the number of cross-linking points.[37] Consequently, higher thermal energy is required to enable entropy-driven phase transition.

A larger specific surface area is desirable for adsorbents.[38] To assess the specific surface area of our P-NIPMAM, the carbon dioxide (CO_2) adsorption isotherms were measured by conducting the Brunauer−Emmett−Teller (BET) surface area analyses (Figure 2a, also see the Experimental Section). The isotherms exhibit type-I adsorption curves with concavity to the relative pressure (P/P_0, i.e., pressure of adsorbate (CO_2) divided by its saturation pressure), indicating that P-NIPMAMs possess a microporous (i.e., pore size <2.0 nm)[39] structure.[40] We also found that P-NIPMAM prepared with a higher cross-linker concentration exhibits a higher BET surface area. For example, the BET surface area was measured as ≈90, ≈109, ≈114, ≈156, ≈184, and ≈187 m^2 g^{-1} for P-NIPMAM prepared with 12.5, 25.0, 50.0, 75.0, 100.0, and 125.0 wt % of cross-linker concentration, respectively (Figure 2b). An increase in the BET surface area with a higher cross-linker concentration can be attributed to a more rigid structure that can prevent entanglement and tight packing of the P-NIPMAM structure.[41]

We measured the adsorption capacity (α, i.e., adsorbed mass per gram of adsorbent) of our P-NIPMAMs with varied BET surface area values for PFASs. Here, PFOA was utilized as a representative PFAS. A cross-linked P-NIPMAM adsorbent (20 mm × 20 mm, thickness = 100 μm) was submerged in a PFOA aqueous solution (concentration, C_o = 0.6 mg mL^{-1}) for 10 h at a temperature of 75 °C (>LCST ≈73.9 °C). Note that the thickness of 100 μm is comparable to that of the adsorbents in PFAS-adsorbing devices (e.g., Polar Organic Chemical Integrative Sampler modules) that are currently in use.[42,43] Figure 2c demonstrates the value of α which is given by $\alpha = (C_o - C_{a,t=10h})V/m$.[44] Here, $C_{a,t=10h}$ is the concentration of PFOA at t = 10 h. V and m are the volume of the PFOA solution (20 mL) and the mass of dry P-NIPMAM (100 mg), respectively. High-performance liquid chromatography−mass spectrometry (HPLC-MS) was utilized to measure $C_{a,t}$ (Experimental Section). The results show that P-NIPMAM with a larger BET surface area exhibits a higher value of α indicating that it can adsorb and retain more PFOA. For example, P-NIPMAM with 90 m^2 g^{-1} of BET surface area exhibits $\alpha \approx$ 12 mg g^{-1} (i.e., 12 mg of PFOA adsorption per 1 g of P-NIPMAM), while that with 156 m^2 g^{-1} BET surface area exhibits $\alpha \approx$ 37 mg g^{-1}. Please note that the α values remain almost constant after ≈10 h of immersion indicating that the equilibrium condition (i.e., α_{max}, the maximum adsorption capacity) was attained. Of note, the α_{max} values remained almost constant when the BET surface area becomes greater than 156 m^2 g^{-1}. Thus, the P-NIPMAM with 156 m^2 g^{-1} BET surface area was utilized for the rest of this study. The α_{max} values were also measured for sodium dodecyl sulfate (SDS) which is a nonfluorinated anionic molecule (Supporting Information, Section 1).

Adsorption of PFOA is primarily driven by the hydrophobic interaction between the fluoroalkyl chain of PFOA and P-NIPMAM's isopropyl or methyl groups when a temperature is above the LCST (Scheme 1). When the temperature becomes lower than the LCST, P-NIPMAM retrieves a coil-like conformation with the extended amide groups that can hydrogen-bond with water.[31,32] This can result in the desorption of PFOA. Such LCST-driven adsorption and desorption cycles are reversible.[45]

Scheme 1. Schematic Demonstrating the Adsorption of PFASs (e.g., PFOA) by P-NIPMAM via Hydrophobic Interaction between the Fluoroalkyl Chain of PFASs and Hydrophobes of the P-NIPMAM (e.g., Isopropyl and/or Methyl) at T > LCST[a]

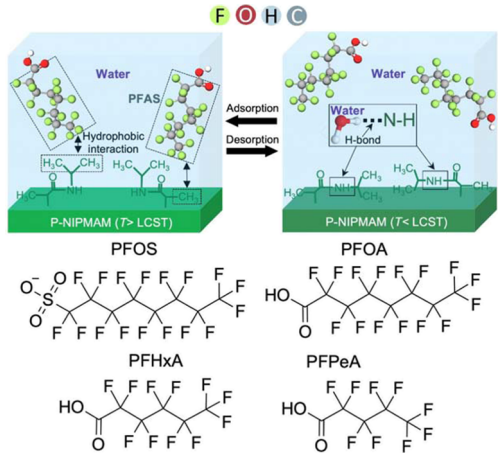

[a]When the temperature is below the LCST, the P-NIPMAM retrieves coil-like conformation to expose hydrophilic amide groups leading to desorption of PFASs and hydrogen bonding with surrounding water molecules.

The kinetics of adsorption and desorption of PFASs to our P-NIPMAM was investigated. Here, four PFASs with varied fluoroalkyl chain lengths were utilized that include PFOA ($(CF_2)_6-CF_3$), PFHxA ($(CF_2)_4-CF_3$), and perfluoropentanoic acid (PFPeA, $(CF_2)_3-CF_3$). In addition, PFOS [$(CF_2)_7-$

https://doi.org/10.1021/acsapm.1c00608
ACS Appl. Polym. Mater. 2021, 3, 4139−4146

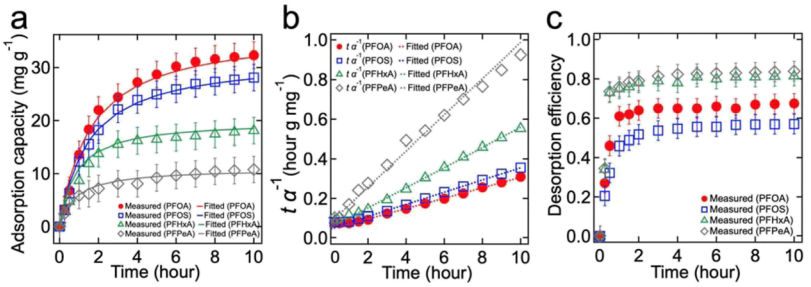

Figure 3. (a) Measured adsorption capacity for PFPeA, PFHxA, PFOA, and PFOS in water (C_o = 0.6 mg mL^{-1}) as a function of immersion time at $T \approx 75$ °C. The predicted values obtained by utilizing the pseudo-second-order kinetic model (eq 1) are also shown for comparison. (b) Plots of the values of $t\alpha^{-1}$ for PFPeA, PFHxA, PFOA, and PFOS as a function of immersion time.The intercept of the fitted lines with the y-axis was utilized to determine the values of k_2. (c) Measured desorption efficiency for PFPeA, PFHxA, PFOA, and PFOS at $T \approx 23$ °C.

(CF_3)] was also used which has a long fluoroalkyl chain (e.g., PFOA), while it possesses a sulfonic acid functional group. This will enable us to investigate the effect of a functional group on the adsorption or desorption kinetics.

First, the adsorption capacity was measured at T = 75 °C (>LCST) (Figure 3a). Of note, the concentration (C_o) for all PFAS solutions was 0.6 mg mL^{-1} which is far below the critical micelle concentration for PFASs used here [e.g., ≈4.5 mg mL^{-1} (PFOS), ≈10.3 mg mL^{-1} (PFOA), ≈28.0 mg mL^{-1} (PFHxA), and ≈66.0 mg mL^{-1} (PFPeA)].[46−48] This is critical to accurate measurements because the PFAS adsorption can be decreased by micelle formation.[49] The results show that PFASs with a longer fluoroalkyl chain exhibit a higher value of α_{max}. For example, theα_{max} values were ≈11, ≈18, and ≈37 for PFPeA, PFHxA, and PFOA, respectively. This can be attributed to the fact that a longer fluoroalkyl chain can constitute a stronger hydrophobic interaction[4,50,51] with the hydrophobes of the P-NIPMAM (i.e., isopropyl and/or methyl groups) and show a lower water solubility (e.g., 9.5 mg mL^{-1} for PFOA) than that with a shorter fluoroalkyl chain (e.g., 15.7 mg mL^{-1} for PFHxA). This can result in a decrease in the partitioning in water and facilitates adsorption to the P-NIPMAM.[14,51] Interestingly, the α_{max} value for PFOS was measured as ≈32 mg g^{-1} which is lower than that of PFOA (≈37 mg g^{-1}), although it possesses a slightly longer fluoroalkyl chain (i.e., $(CF_2)_7$−CF_3). This can be attributed to a sulfonate group of PFOS which can form a stronger hydrogen bond with water and impede the adsorption in comparison with a carboxylate group in PFOA.[24] Of note, the concentration of PFAS in water ($C_{a,t}$) was determined by measuring the electrical conductivity of a solution and comparing the value with the calibration curves (Supporting Information Section 2). The concentration of a solution at equilibrium ($C_{a,t=10h}$) was further verified by HPLC-MS (Experimental Section and Supporting Information Section 3).

The PFAS adsorption to the P-NIPMAM surface is a kinetic process that can be described by a pseudo-second-order kinetic model. The adsorption capacity (α) is given as[52−55]

$$\alpha = (k_2 {\alpha_{max}}^2 t/(1 + k_2 \alpha_{max} t)) \quad (1)$$

where α_{max} and k_2 are the maximum adsorption capacity and the adsorption rate constant, respectively. The approximate values of k_2 were determined by plotting $t\alpha^{-1}$ against t and utilizing the intercept of the fitted lines with the y-axis (Figure 3b and Table 1).[56−58] The results show that the adsorption rate for a PFAS with a longer fluoroalkyl chain (e.g., PFOA) is higher than that of PFAS with a shorter chain (e.g., PFPeA). A lower value of the initial adsorption rate for PFOS compared to that of PFOA can be attributed to its larger molar mass which can pose a steric effect.[59] Please note that the initial adsorption rate (ϑ, i.e., fast initial adsorption due to a large concentration gradient) of various PFASs can be determined by calculating the value of $\vartheta = k_2 {\alpha_{max}}^2$.[24] The values of ϑ are also listed in Table 1.

Table 1. Values of the Adsorption Rate Constant (k_2) and the Initial Adsorption Rate (ϑ) for Various PFASs

PFAS	k_2 (g mg^{-1} h^{-1})	ϑ (mg g^{-1} h^{-1})
PFOS	0.021	21.6
PFOA	0.017	23.5
PFHxA	0.061	20.0
PFPeA	0.111	13.4

Release of the adsorbed PFAS on demand is critical to both regenerating the adsorbent for reuse and concentrating the PFAS in a sampling solvent. The release test was conducted by submerging the P-NIPMAM in DI water (volume = 20 mL) at ≈23 °C (i.e., below LCST). Note that the P-NIPMAM that has attained the maximum adsorption capacity for a given PFAS was utilized. The desorption efficiency (ξ_d) was calculated by[60,61]

$$\xi_d = C_{d,t}/(C_o - C_{a,t=10h}) \quad (2)$$

where $C_{d,t}$ is the concentration of the PFAS in DI water at time t during the test. The values of ξ_d remained almost unchanged after ≈8 h indicating that the equilibrium condition is attained (i.e., $\xi_{d.max}$, the maximum desorption efficiency) (Figure 3c). The $\xi_{d.max}$ values were measured as ≈0.83, ≈0.81, ≈0.66, and ≈0.57 for PFPeA, PFHxA, PFOA, and PFOS, respectively. This can be a direct consequence of a weaker hydrophobic interaction of PFASs with a shorter fluoroalkyl chain (e.g., PFPeA) which can result in a facile release in comparison with that with a longer chain (e.g., PFOA). The concentration of a solution was determined by electrical conductivity measurements and the HPLC-MS method (also see Supporting Information Section 3). Similar to the adsorption kinetics, desorption of PFASs can be described using a pseudo-second-order kinetic model (Supporting Information Section 4).

Finally, a prototype device was engineered that can adsorb, retain, and release PFASs upon switching the temperature (Figure 4a, also see the Experimental Section). The device was fabricated by coating open-channel support (polyethylene, 140 mm × 40 mm) with our P-NIPMAM (thickness of ≈100 μm). The whole device was tilted at an angle of 30° with reference to the horizontal plane so that the injected PFAS solution can flow through the channel under gravitational force. Approx-

https://doi.org/10.1021/acsapm.1c00608
ACS Appl. Polym. Mater. 2021, 3, 4139−4146

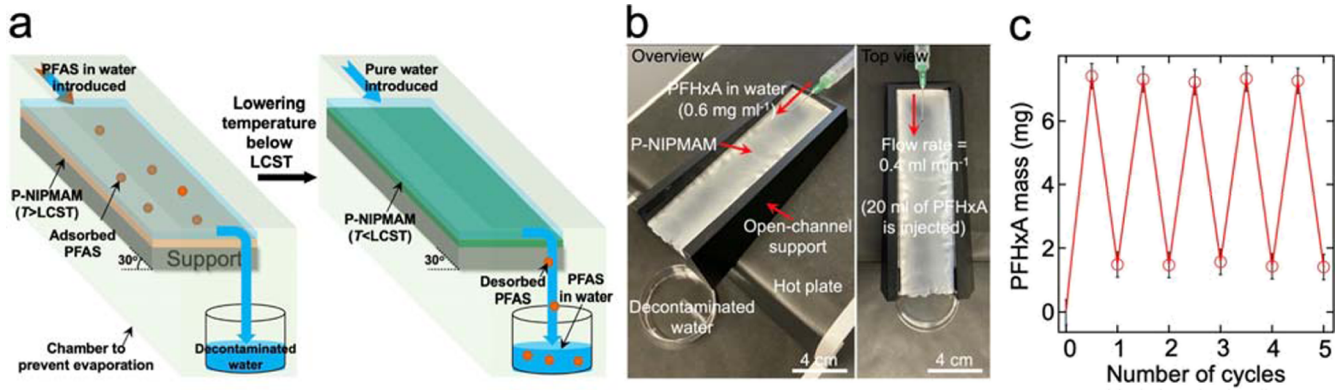

Figure 4. (a) Schematic and (b) photograph showing the working principle of a P-NIPMAM prototype device utilized for the LCST-driven adsorption and desorption of PFHxA. (c) Plot of the adsorbed and desorbed mass of PFHxA upon repeated adsorption−desorption cycles (five cycles).

imately, 20 mL of PFHxA solution (C_o = 0.6 mg mL^{-1}, a total PFHxA = 12 mg) was continuously fed into the channel with a constant flow rate of 0.4 mL min^{-1} using a syringe pump (Figure 4b). The temperature of the P-NIPMAM surface was maintained at $T \approx 75$ °C (>LCST). The solution was collected at the outlet of the channel. The concentration of PFHxA was determined by the electrical conductivity measurements and the HPLC-MS method. It was measured as ≈0.23 mg mL^{-1} indicating that ≈7.4 mg of PFHxA was adsorbed by P-NIPMAM. Please note that the absorption of the solution by P-NIPMAM was negligible (<0.01 mL).

The PFHxA release test was conducted by feeding DI water (20 mL) to the channel with a flow rate of 0.4 mL min^{-1}, while the P-NIPMAM temperature was maintained at T = 23 °C (<LCST). The concentration of PFHxA in DI water was measured as ≈0.29 mg mL^{-1} which is equivalent to a desorption efficiency, $\xi_d \approx 0.80$. Please note that the adsorption−desorption cycles can be repeated (Figure 4c). Our P-NIPMAM is also effective in adsorbing and releasing a commercial fluoro-surfactant (Capstone FS-66, Supporting Information Sections 5 and 6) upon temperature change.

CONCLUSIONS

In this work, thermoresponsive P-NIPMAM was synthesized that can adsorb and retain PFASs at a temperature higher than the LCST while releasing them at a lower temperature. The PFOA and PFHxA were utilized as representative PFASs with a long and short fluoroalkyl chain, respectively. The adsorption capacity for PFOA and PFHxA was measured as ≈37 and ≈18 mg g^{-1} at 75 °C, respectively. When the P-NIPMAM was submerged in DI water at a temperature lower than the LCST, it started to release the adsorbed compounds resulting in the desorption efficiency of ≈0.66 and ≈0.81 for PFOA and PFHxA, respectively. This can be attributed to a stronger hydrophobic interaction between the hydrophobes of the P-NIPMAM (i.e., isopropyl and/or methyl groups) and a longer fluoroalkyl chain. It was also demonstrated that PFAS adsorption and desorption kinetics can be described using a pseudo-second-order kinetic model. Finally, a prototype PFAS sampler was engineered by utilizing P-NIPMAM that can demonstrate the LCST-driven reversible adsorption and desorption of PFASs.

EXPERIMENTAL SECTION

Synthesis of P-NIPMAM. A solution of NIPMAM monomer, MBAA (cross-linker), and KPS (initiator) was prepared in a water/ethanol mixture (80:20 vol/vol). The overall concentration of the solute (i.e., NIPMAM, MBAA, and KPS) was 25 wt %. The concentration of the cross-linker was 12.5, 25.0, 50.0, 75.0, and 100.0 wt % with respect to the NIPMAM monomer. The concentration of the initiator was 5.0 wt % with respect to the NIPMAM monomer and the cross-linker. The solution was cast in a Petridish. Free-radical polymerization was performed at 70 °C for 1 h to fabricate P-NIPMAM with ≈100 μm thickness. The resulting P-NIPMAM was rinsed several times with DI water to remove unreacted monomers, followed by drying in a vacuum oven at 70 °C for 3 h. Subsequently, the P-NIPMAM was cut into 20 mm × 20 mm squares for the experiments.

High-Performance Liquid Chromatography−Mass Spectrometry. HPLC-MS was conducted by utilizing QTRAP 6500. The mobile phase was HPLC-grade methanol. A total of 20 μL of the samples (i.e., PFAS in DI water) was injected at a flow rate of 200 μL min^{-1}, and the temperature of the column was maintained at 25 °C.

Differential Scanning Calorimetry. Calorimetric investigations in DI water were conducted by heating approximately 10 mg of P-NIPMAM from 0 to 90 °C at a heating rate of 5 °C min^{-1} by utilizing a TA Instruments Q200 differential scanning calorimeter. Please note that helium gas at a flow rate of 20 mL min^{-1} was utilized during DSC measurements.

Surface Area Analysis. A TriStar II 3020 surface analyzer was utilized to determine the BET surface area. The adsorption isotherms of carbon dioxide (CO_2) were measured at a temperature of 273 °K.

Scanning Electron Microscopy. The morphology and surface texture of P-NIPMAM were characterized by utilizing a field emission scanning electron microscope (FEI Versa 3D DualBeam) at an accelerating voltage of 10 kV. The surface of P-NIPMAM was sputter-coated with a thin layer of gold (≈4−5 nm) to minimize charging.

FTIR Analysis. A PerkinElmer Spectrum 400 FTIR spectrometer was utilized in the attenuated total reflectance mode in the range of 600−4000 cm^{-1}. The FTIR spectra were recorded at a resolution of 4 cm^{-1} for 16 scans.

UV−Vis Analysis. Ultraviolet−visible (UV−Vis) spectrophotometry was conducted by utilizing a Thermo Evolution 600 UV/visible spectrophotometer at a scan speed of 240 nm min^{-1} with a data interval of 2 nm.[62] Please note that the spectrum of acetone was utilized as the background during UV−vis measurements.

ASSOCIATED CONTENT

Supporting Information

The Supporting Information is available free of charge at https://pubs.acs.org/doi/10.1021/acsapm.1c00608.

https://doi.org/10.1021/acsapm.1c00608
ACS Appl. Polym. Mater. 2021, 3, 4139−4146

Maximum adsorption capacity of P-NIPMAM submerged in SDS solution, PFAS concentration calibration curves, HPLC-MS analyses, describing the desorption efficiency for PFASs using a pseudo-second-order kinetic model, UV−vis absorption spectra and the concentration calibration curve for Capstone FS-66, and adsorption and desorption of a fluoro-surfactant by P-NIPMAM (PDF)

AUTHOR INFORMATION

Corresponding Author

Gibum Kwon − *Department of Mechanical Engineering, University of Kansas, Lawrence, Kansas 66045, United States;* orcid.org/0000-0002-7192-1910; Email: gbkwon@ku.edu

Authors

Mohammadamin Ezazi − *Department of Mechanical Engineering, University of Kansas, Lawrence, Kansas 66045, United States;* orcid.org/0000-0003-2284-9809

Bishwash Shrestha − *Department of Mechanical Engineering, University of Kansas, Lawrence, Kansas 66045, United States;* orcid.org/0000-0003-0045-8890

Complete contact information is available at: https://pubs.acs.org/10.1021/acsapm.1c00608

Author Contributions

M.E. and B.S. equally contributed to this work. M.E. and B.S. performed the experiments, analyzed data, and wrote the manuscript. G.K. conceived the project, designed the experiments, and wrote the manuscript.

Notes

The authors declare no competing financial interest.

ACKNOWLEDGMENTS

This research was supported by the National Science Foundation [award number: CBET-1944314] and NASA Kansas EPSCoR [award number: R52123-20-02314].

REFERENCES

(1) Maimaiti, A.; Deng, S.; Meng, P.; Wang, W.; Wang, B.; Huang, J.; Wang, Y.; Yu, G. Competitive Adsorption of Perfluoroalkyl Substances on Anion Exchange Resins in Simulated Afff-Impacted Groundwater. *Chem. Eng. J.* **2018**, *348*, 494−502.

(2) Moody, C. A.; Field, J. A. Perfluorinated Surfactants and the Environmental Implications of Their Use in Fire-Fighting Foams. *Environ. Sci. Technol.* **2000**, *34*, 3864−3870.

(3) Li, Z.; Rabnawaz, M.; Khan, B. Response Surface Methodology Design for Biobased and Sustainable Coatings for Water- and Oil-Resistant Paper. *ACS Appl. Polym. Mater.* **2020**, *2*, 1378−1387.

(4) Gagliano, E.; Sgroi, M.; Falciglia, P. P.; Vagliasindi, F. G. A.; Roccaro, P. Removal of poly- and perfluoroalkyl substances (PFAS) from water by adsorption: Role of PFAS chain length, effect of organic matter and challenges in adsorbent regeneration. *Water Res.* **2020**, *171*, 115381.

(5) Han, H.-C.; Tseng, C.-A.; Du, C.-Y.; Ganguly, A.; Chong, C.-W.; Wang, S.-B.; Lin, C.-F.; Chang, S.-H.; Su, C.-C.; Lee, J.-H.; Chen, K.-H.; Chen, L.-C. Enhancing Efficiency with Fluorinated Interlayers in Small Molecule Organic Solar Cells. *J. Mater. Chem.* **2012**, *22*, 22899−22905.

(6) Zaggia, A.; Conte, L.; Falletti, L.; Fant, M.; Chiorboli, A. Use of Strong Anion Exchange Resins for the Removal of Perfluoroalkylated Substances from Contaminated Drinking Water in Batch and Continuous Pilot Plants. *Water Res.* **2016**, *91*, 137−146.

(7) Backe, W. J.; Day, T. C.; Field, J. A. Zwitterionic, Cationic, and Anionic Fluorinated Chemicals in Aqueous Film Forming Foam Formulations and Groundwater from U.S. Military Bases by Nonaqueous Large-Volume Injection HPLC-MS/MS. *Environ. Sci. Technol.* **2013**, *47*, 5226−5234.

(8) Darlington, R.; Barth, E.; McKernan, J. The Challenges of Pfas Remediation. *Mil. Eng.* **2018**, *110*, 58−60.

(9) Daly, E. R.; Chan, B. P.; Talbot, E. A.; Nassif, J.; Bean, C.; Cavallo, S. J.; Metcalf, E.; Simone, K.; Woolf, A. D. Per- and Polyfluoroalkyl Substance (Pfas) Exposure Assessment in a Community Exposed to Contaminated Drinking Water, New Hampshire, 2015. *Int. J. Hyg. Environ. Health* **2018**, *221*, 569−577.

(10) Zareitalabad, P.; Siemens, J.; Hamer, M.; Amelung, W. Perfluorooctanoic acid (PFOA) and perfluorooctanesulfonic acid (PFOS) in surface waters, sediments, soils and wastewater—A review on concentrations and distribution coefficients. *Chemosphere* **2013**, *91*, 725−732.

(11) Moreton, J. C.; Palomba, J. M.; Cohen, S. M. Liquid-Phase Applications of Metal-Organic Framework Mixed-Matrix Membranes Prepared from Poly(ethylene-co-vinyl acetate). *ACS Appl. Polym. Mater.* **2020**, *2*, 2063−2069.

(12) Schaider, L. A.; Balan, S. A.; Blum, A.; Andrews, D. Q.; Strynar, M. J.; Dickinson, M. E.; Lunderberg, D. M.; Lang, J. R.; Peaslee, G. F. Fluorinated Compounds in U.S. Fast Food Packaging. *Environ. Sci. Technol. Lett.* **2017**, *4*, 105−111.

(13) U.S. Environmental Protection Agency. Draft Contaminant Candidate List 4-CCL 4; U.S.; Environmental Protection Agency: Washington, DC, 2015. http://www.epa.gov/ccl/chemical-contaminants-ccl-4 (accessed Nov 1, 2016).

(14) Park, M.; Wu, S.; Lopez, I. J.; Chang, J. Y.; Karanfil, T.; Snyder, S. A. Adsorption of Perfluoroalkyl Substances (Pfas) in Groundwater by Granular Activated Carbons: Roles of Hydrophobicity of Pfas and Carbon Characteristics. *Water Res.* **2020**, *170*, 115364.

(15) Rodriguez, K. L.; Hwang, J.-H.; Esfahani, A. R.; Sadmani, A. H. M. A.; Lee, W. H. Recent Developments of Pfas-Detecting Sensors and Future Direction: A Review. *Micromachines* **2020**, *11*, 667.

(16) Fang, C.; Zhang, X.; Dong, Z.; Wang, L.; Megharaj, M.; Naidu, R. Smartphone App-Based/Portable Sensor for the Detection of Fluoro-Surfactant Pfoa. *Chemosphere* **2018**, *191*, 381−388.

(17) Salihović, S.; Dickens, A. M.; Schoultz, I.; Fart, F.; Sinisalu, L.; Lindeman, T.; Halfvarson, J.; Orešič, M.; Hyötyläinen, T. Simultaneous determination of perfluoroalkyl substances and bile acids in human serum using ultra-high-performance liquid chromatography-tandem mass spectrometry. *Anal. Bioanal. Chem.* **2020**, *412*, 2251−2259.

(18) Boone, J. S.; Vigo, C.; Boone, T.; Byrne, C.; Ferrario, J.; Benson, R.; Donohue, J.; Simmons, J. E.; Kolpin, D. W.; Furlong, E. T.; Glassmeyer, S. T. Per- and polyfluoroalkyl substances in source and treated drinking waters of the United States. *Sci. Total Environ.* **2019**, *653*, 359−369.

(19) Zhang, X.; Niu, H.; Pan, Y.; Shi, Y.; Cai, Y. Chitosan-Coated Octadecyl-Functionalized Magnetite Nanoparticles: Preparation and Application in Extraction of Trace Pollutants from Environmental Water Samples. *Anal. Chem.* **2010**, *82*, 2363−2371.

(20) Xia, W.; Wan, Y.-J.; Wang, X.; Li, Y.-y.; Yang, W.-J.; Wang, C.-X.; Xu, S.-q. Sensitive bioassay for detection of PPARα potentially hazardous ligands with gold nanoparticle probe. *J. Hazard. Mater.* **2011**, *192*, 1148−1154.

(21) Chen, S.; Li, A.; Zhang, L.; Gong, J. Molecularly imprinted ultrathin graphitic carbon nitride nanosheets-Based electrochemiluminescence sensing probe for sensitive detection of perfluorooctanoic acid. *Anal. Chim. Acta* **2015**, *896*, 68−77.

(22) Chen, L. D.; Lai, C.-Z.; Granda, L. P.; Fierke, M. A.; Mandal, D.; Stein, A.; Gladysz, J. A.; Bühlmann, P. Fluorous Membrane Ion-Selective Electrodes for Perfluorinated Surfactants: Trace-Level Detection and in Situ Monitoring of Adsorption. *Anal. Chem.* **2013**, *85*, 7471−7477.

(23) Ateia, M.; Arifuzzaman, M.; Pellizzeri, S.; Attia, M. F.; Tharayil, N.; Anker, J. N.; Karanfil, T. Cationic Polymer for Selective Removal

of Genx and Short-Chain Pfas from Surface Waters and Wastewaters at Ng/L Levels. *Water Res.* **2019**, *163*, 114874.
(24) Saad, A.; Mills, R.; Wan, H.; Mottaleb, M. A.; Ormsbee, L.; Bhattacharyya, D. Thermo-Responsive Adsorption-Desorption of Perfluoroorganics from Water Using Pnipam Hydrogels and Pore Functionalized Membranes. *J. Membr. Sci.* **2020**, *599*, 117821.
(25) Xiang, J.; Zheng, W.; Yan, J.; Liang, X.; Zhang, H.; Liu, B.; Zou, W. Thermally Driven Separation of Perfluoroalkyl Substances with High Efficiency. *ACS Appl. Mater. Interfaces* **2020**, *12*, 40759−40767.
(26) Bonham, J. A.; Waggett, F.; Faers, M. A.; Van Duijneveldt, J. S. The Role of Initiator on the Dispersibility of Polystyrene Microgels in Non-Aqueous Solvents. *Colloid Polym. Sci.* **2017**, *295*, 479−486.
(27) Futscher, M. H.; Philipp, M.; Müller-Buschbaum, P.; Schulte, A. The Role of Backbone Hydration of Poly(N-isopropyl acrylamide) Across the Volume Phase Transition Compared to its Monomer. *Sci. Rep.* **2017**, *7*, 17012.
(28) Maeda, Y.; Nakamura, T.; Ikeda, I. Changes in the Hydration States of Poly(N-n-propylmethacrylamide) and Poly(N-isopropylmethacrylamide) during Their Phase Transitions in Water Observed by FTIR Spectroscopy. *Macromolecules* **2001**, *34*, 8246−8251.
(29) Evanghelidis, A.; Beregoi, M.; Diculescu, V. C.; Galatanu, A.; Ganea, P.; Enculescu, I. Flexible Delivery Patch Systems Based on Thermoresponsive Hydrogels and Submicronic Fiber Heaters. *Sci. Rep.* **2018**, *8*, 17555.
(30) Kurečič, M.; Sfiligoj-Smole, M.; Stana-Kleinschek, K. Uv Polymerization of Poly (N-Isopropylacrylamide) Hydrogel. *Mater. Tehnol.* **2012**, *46*, 87−91.
(31) Deshmukh, S. A.; Sankaranarayanan, S. K. R. S.; Suthar, K.; Mancini, D. C. Role of Solvation Dynamics and Local Ordering of Water in Inducing Conformational Transitions in Poly(N-isopropylacrylamide) Oligomers through the LCST. *J. Phys. Chem. B* **2012**, *116*, 2651−2663.
(32) Singh, R.; Deshmukh, S. A.; Kamath, G.; Sankaranarayanan, S. K. R. S.; Balasubramanian, G. Controlling the Aqueous Solubility of Pnipam with Hydrophobic Molecular Units. *Comput. Mater. Sci.* **2017**, *126*, 191−203.
(33) Salmerón Sánchez, M.; Hanyková, L.; Ilavský, M.; Monleón Pradas, M. Thermal transitions of poly(N-isopropylmethacrylamide) in aqueous solutions. *Polymer* **2004**, *45*, 4087−4094.
(34) Maharjan, A.; Ezazi, M.; Kwon, G. Hydrogel with Selective Absorption for Separation of Liquid Mixtures. U.S. Patent 20,200,399,430 A1, 2020.
(35) Yim, H.; Kent, M. S.; Mendez, S.; Balamurugan, S. S.; Balamurugan, S.; Lopez, G. P.; Satija, S. Temperature-Dependent Conformational Change of Pnipam Grafted Chains at High Surface Density in Water. *Macromolecules* **2004**, *37*, 1994−1997.
(36) Wu, T.-Y.; Zrimsek, A. B.; Bykov, S. V.; Jakubek, R. S.; Asher, S. A. Hydrophobic Collapse Initiates the Poly(N-isopropylacrylamide) Volume Phase Transition Reaction Coordinate. *J. Phys. Chem. B* **2018**, *122*, 3008−3014.
(37) Kratz, K.; Hellweg, T.; Eimer, W. Structural Changes in Pnipam Microgel Particles as Seen by Sans, Dls, and Em Techniques. *Polymer* **2001**, *42*, 6631−6639.
(38) Cossu, R.; Ehrig, H.-J.; Muntoni, A. Physical-Chemical Leachate Treatment. In *Solid Waste Landfilling*; Cossu, R., Stegmann, R., Eds.; Elsevier, 2018; Chapter 10.4, pp 575−632.
(39) Zhao, J.; Yan, W. Microwave-Assisted Inorganic Syntheses. In *Modern Inorganic Synthetic Chemistry*; Xu, R., Pang, W., Huo, Q., Eds.; Elsevier: Amsterdam, 2011; Chapter 8 pp 173−195.
(40) Rouquerol, J.; Rouquerol, F.; Sing, K. S. W. *Adsorption by Powders and Porous Solids: Principles, Methodology and Applications*; Elsevier Science, 1998; pp 19−181.
(41) Wu, S.; Gu, S.; Zhang, A.; Yu, G.; Wang, Z.; Jian, J.; Pan, C. A rational construction of microporous imide-bridged covalent-organic polytriazines for high-enthalpy small gas absorption. *J. Mater. Chem. A* **2015**, *3*, 878−885.
(42) Kaserzon, S. L.; Hawker, D. W.; Kennedy, K.; Bartkow, M.; Carter, S.; Booij, K.; Mueller, J. F. Characterisation and Comparison of the Uptake of Ionizable and Polar Pesticides, Pharmaceuticals and Personal Care Products by Pocis and Chemcatchers. *Environ. Sci.: Processes Impacts* **2014**, *16*, 2517−2526.
(43) Cerveny, D.; Grabic, R.; Fedorova, G.; Grabicova, K.; Turek, J.; Kodes, V.; Golovko, O.; Zlabek, V.; Randak, T. Perfluoroalkyl Substances in Aquatic Environment-Comparison of Fish and Passive Sampling Approaches. *Environ. Res.* **2016**, *144*, 92−98.
(44) Udoetok, I. A.; Faye, O.; Wilson, L. D. Adsorption of Phosphate Dianions by Hybrid Inorganic-Biopolymer Polyelectrolyte Complexes: Experimental and Computational Studies. *ACS Appl. Polym. Mater.* **2020**, *2*, 899−910.
(45) Morris, C.; Szczupak, B.; Klymchenko, A. S.; Ryder, A. G. Study of Water Adsorption in Poly(N-isopropylacrylamide) Thin Films Using Fluorescence Emission of 3-Hydroxyflavone Probes. *Macromolecules* **2010**, *43*, 9488−9494.
(46) Shih, K.; Wang, F. Adsorption Behavior of Perfluorochemicals (Pfcs) on Boehmite: Influence of Solution Chemistry. *Procedia Environ. Sci.* **2013**, *18*, 106−113.
(47) Alves, A. V.; Tsianou, M.; Alexandridis, P. Fluorinated Surfactant Adsorption on Mineral Surfaces: Implications for Pfas Fate and Transport in the Environment. *Surfaces* **2020**, *3*, 516−566.
(48) Karnwadee, W. Development of Effective Removal Procedures of Perfluorohexanoic Acid (Pfhxa) from Industrial Wastewater by Adsorption and Regeneration. Ph.D. Dissertation, Kyoto University, Kyoto, Japan, 2015.
(49) Deng, S.; Niu, L.; Bei, Y.; Wang, B.; Huang, J.; Yu, G. Adsorption of Perfluorinated Compounds on Aminated Rice Husk Prepared by Atom Transfer Radical Polymerization. *Chemosphere* **2013**, *91*, 124−130.
(50) Li, F.; Duan, J.; Tian, S.; Ji, H.; Zhu, Y.; Wei, Z.; Zhao, D. Short-chain per- and polyfluoroalkyl substances in aquatic systems: Occurrence, impacts and treatment. *Chem. Eng. J.* **2020**, *380*, 122506.
(51) Du, Z.; Deng, S.; Bei, Y.; Huang, Q.; Wang, B.; Huang, J.; Yu, G. Adsorption behavior and mechanism of perfluorinated compounds on various adsorbents-A review. *J. Hazard. Mater.* **2014**, *274*, 443−454.
(52) Xiao, Y.; Azaiez, J.; Hill, J. M. Erroneous Application of Pseudo-Second-Order Adsorption Kinetics Model: Ignored Assumptions and Spurious Correlations. *Ind. Eng. Chem. Res.* **2018**, *57*, 2705−2709.
(53) Ho, Y. S.; McKay, G. Pseudo-Second Order Model for Sorption Processes. *Process Biochem.* **1999**, *34*, 451−465.
(54) Li, W.-T.; Zhuang, Y.-T.; Wang, J.-Y.; Yang, T.; Yu, Y.-L.; Chen, M.-L.; Wang, J.-H. A Three-Dimensional Porous Organic Framework for Highly Selective Capture of Mercury and Copper Ions. *ACS Appl. Polym. Mater.* **2019**, *1*, 2797−2806.
(55) Süslükaya, M.; Mumcu Topaloğlu, H.; Gül Karagüler, N.; Yavuz, E. Hierarchically Porous High-Surface-Area Polymers with Interconnected Pores for Fast and Selective Albumin Adsorption. *ACS Appl. Polym. Mater.* **2021**, *3*, 2742−2758.
(56) Barathi, M.; Santhana Krishna Kumar, A.; Rajesh, N. Efficacy of novel Al-Zr impregnated cellulose adsorbent prepared using microwave irradiation for the facile defluoridation of water. *J. Environ. Chem. Eng.* **2013**, *1*, 1325−1335.
(57) Lu, T.; Xiang, T.; Huang, X.-L.; Li, C.; Zhao, W.-F.; Zhang, Q.; Zhao, C.-S. Post-Crosslinking Towards Stimuli-Responsive Sodium Alginate Beads for the Removal of Dye and Heavy Metals. *Carbohydr. Polym.* **2015**, *133*, 587−595.
(58) Bhatnagar, A.; Kumar, E.; Minocha, A. K.; Jeon, B.-H.; Song, H.; Seo, Y.-C. Removal of Anionic Dyes from Water usingCitrus limonum(Lemon) Peel: Equilibrium Studies and Kinetic Modeling. *Sep. Sci. Technol.* **2009**, *44*, 316−334.
(59) Du, Z.; Deng, S.; Chen, Y.; Wang, B.; Huang, J.; Wang, Y.; Yu, G. Removal of Perfluorinated Carboxylates from Washing Wastewater of Perfluorooctanesulfonyl Fluoride Using Activated Carbons and Resins. *J. Hazard. Mater.* **2015**, *286*, 136−143.
(60) El Boujaady, H.; Mourabet, M.; Bennani-Ziatni, M.; Taitai, A. Adsorption/Desorption of Direct Yellow 28 on Apatitic Phosphate: Mechanism, Kinetic and Thermodynamic Studies. *J. Assoc. Arab Univ. Basic Appl. Sci.* **2014**, *16*, 64−73.

https://doi.org/10.1021/acsapm.1c00608
ACS Appl. Polym. Mater. 2021, 3, 4139−4146

(61) Momina; Mohammad, S.; Suzylawati, I. Study of the Adsorption/Desorption of Mb Dye Solution Using Bentonite Adsorbent Coating. *J. Water Process Eng.* **2020**, *34*, 101155.
(62) Qahtan, T. F.; Gondal, M. A.; Dastageer, M. A.; Kwon, G.; Ezazi, M.; Al-Kuban, M. Z. Thermally Sensitized Membranes for Crude Oil-Water Remediation under Visible Light. *ACS Appl. Mater. Interfaces* **2020**, *12*, 48572−48579.

https://doi.org/10.1021/acsapm.1c00608
ACS Appl. Polym. Mater. 2021, 3, 4139−4146